(Received 8 October 2024, Accepted 3 December 2024, Scheduled 29 December 2024)

Magneto-Acousto-Electrical Tomography Method for Conductivity Reconstruction of Complex Structural Models

Di Fan[1], Xingchen Zhang[1, 2, 4], Yuanyuan Li[2, 3, 4, *], Huiling Liu[2], Jing Liu[2, 3, 4], and Guoqiang Liu[2, 3, 4]

[1] *Shandong University of Science and Technology, Qingdao, China*
[2] *Institute of Electrical Engineering, Chinese Academy of Sciences, Beijing 100190, China*
[3] *School of Electronic Electrical and Communication Engineering University of Chinese Academy of Sciences, Beijing 100049, China*
[4] *Institute of Electrical Engineering and Advanced Electromagnetic Drive Technology, Qilu Zhongke, China*

ABSTRACT: Magneto-Acousto-Electrical Tomography (MAET), as one of the electrical characterization imaging methods, is used to image the electrical conductivity of biological tissues, which can be used for noninvasive, radiation-free imaging of biological tissues. Currently, most of the studies on MAET are simulations and experimental validations of simple structural models, and there is no sufficient validation of models with complex structures. Most of the results cannot comprehensively invert complex structural models with multi-gradient conductivity distributions. To address this problem, this paper proposes a MAET method for conductivity reconstruction of complex structural models which is applicable to 2D problems and may be extendable to 3D problems. Based on this method, the conductivity distribution of normal and diseased tissues in the simulation model of complex structures was reconstructed, and the consistency between experimental and simulated signals was verified. The results show that the MAET method for conductivity reconstruction of complex structural models proposed in this paper is conducive to improving the image resolution as well as the structural similarity, enhancing the conductivity distribution information of complex structural targets with inhomogeneous shapes and multi-gradient conductivity distributions.

1. INTRODUCTION

The incidence and mortality rates of malignant tumors [1] have been increasing globally year by year, and have become a public health problem that poses a major threat to the health of people in China and around the world. Since many malignant tumors have insignificant symptoms in the early stages, prevention and early screening are essential to reduce the morbidity and mortality of malignant tumors. Malignant tumors with complex structures pose certain challenges to early prevention and screening.

Since the electrical properties of biological tissues at the lesion site change with the extent of the lesion [2], electrical characterization imaging methods are expected to achieve early detection of lesions as a new imaging technique. Magneto-Acousto-Electrical Tomography (MAET) [3], as one of the electrical characterization imaging methods, is used to image the electrical conductivity of biological tissues and can be used for noninvasive, radiation-free imaging of biological tissues.

Wen et al. first proposed Hall Effect Imaging (HEI) in 1998, a technique that was initially recognized as having potential as a noninvasive diagnostic tool for assessing the electrical properties of breast cancer and other biological tissues [3]. Subsequently, in 2000, Wen further explored the promise of HEI for biomedical applications [4]. It was pointed out that HEI techniques can effectively map the boundaries between tissues with different conductivities. However, HEI technique has some limitations in providing accurate quantitative images of conductivity and dielectric constant. Nonetheless, the application of HEI techniques in biomedical imaging has shown its unique value, especially in the ability to distinguish between tissues with different electrical properties. Zeng et al. [5] proposed MAET in 2010, which combines conventional electrical impedance imaging and ultrasound imaging. A two-dimensional simple simulation model was computationally analyzed for its MAET signal. Kunyansky in 2012 [6] introduced the mathematical model and inversion process of MAET. Firstly, the mathematical model in MAET measurements was discussed, including the relationship between potential, current and magnetic induction strength. Then, a method for reconstructing tissue conductivity based on measurement data was proposed.

Salim et al. further developed MAET in 2013 [7] and proposed a hybrid magneto-acoustic method for breast cancer detection. In 2016, Zengin et al. [8] introduced the principles and methods of Lorentz force electrical impedance tomography, and a simple square model was used to represent the tumor structure for imaging analysis. In 2020, Sun et al. [9] proposed an improved MAET algorithm to distinguish irregularly shaped tumors at different locations. Double elliptically shaped anomalies and single simple irregular anomalies were set up for imaging validation. In 2023, Jin et nal. introduced the wavelet filtering method into MAET [10]. Based on the Lorentz reciprocity theorem, the fluctuation equation satisfied

* Corresponding author: Yuanyuan Li (lyy@mail.iee.ac.cn).

by the electrode-detectable voltage was derived. An image of the electrical properties of a phantom with a simple structure was realized using the time reversal method, thus reflecting the interface of conductivity changes within the tissue. In 2024, Cheng et al. [11] applied nonlinear frequency modulation (NLFM) ultrasound to MAET to increase the dynamic range of detection and image the conductivity interfaces of ex vivo pork tissues.

Currently, 2D MAET studies are mostly combined with simple structural models for simulation and experimental validation, and models with complex structures are not adequately validated. Although 3D MAET has taken model complexity into account to a larger extent, and the imaging effect for irregularly shaped anomalies is still poor. Most of the results are boundary imaging, which is not able to comprehensively invert the internal conductivity information.

To address the above problems, this paper proposes a MAET method for conductivity reconstruction of complex structural models. Firstly, the principle of MAET is briefly introduced, and then MAET combined with the reciprocity theorem [12] is analyzed to derive the theoretical formula used for MAET. Simulations and experimental validation were carried out based on this relationship, and the simulations were divided into two processes: the actual process and reciprocal process. The conductivity distributions of normal biological tissues and diseased tissues in the simulation model of complex structures are finally reconstructed and compared with the real conductivity distributions as well as the traditional reconstruction methods to verify the advantages of our proposed method. Finally, the consistency between the experimental and simulated signals is experimentally verified. This paper focuses on the imaging of more complex structural models for 2D modeling, and in the future, we will explore specific solutions to improve the imaging of 3D complex models on this basis.

The results show that the MAET method for conductivity reconstruction of complex structural models proposed in this paper is conducive to improving the image resolution as well as the structural similarity, enhancing the conductivity distribution information of complex structural targets with irregular shapes and multi-gradient conductivity distributions.

2. THEORY

2.1. MAET

As shown in Fig. 1, the target body with a conductivity distribution of σ is placed in a static magnetic field $\mathbf{B}_0$, and the ultrasonic pulse excitation is generated by the ultrasonic transducer and acts on the target body, which causes the vibration of the ions in the target body to produce a vibrational velocity $\boldsymbol{\nu}$. The direction of the static magnetic field is along the Z-direction, which is mutually perpendicular to the direction of the pulse, and the vibrating ions are subjected to Lorentz force to produce a charge separation, which generates an equivalent current source [3]:

$$\mathbf{J}_{e1} = \sigma \mathbf{v} \times \mathbf{B}_0 \tag{1}$$

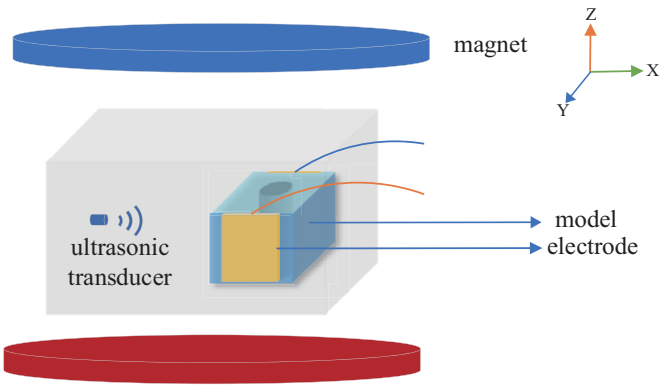

FIGURE 1. Schematic diagram of MAET principle.

In turn, through a pair of detection electrodes on the surface of the target body, the corresponding electrical signals can be extracted, and using the detected electrical signals through certain reconstruction algorithms, it is possible to reconstruct the interface where the conductivity changes.

2.2. Reciprocal Process

The reciprocal process of MAET [12] is to change a pair of measurement electrodes at a_i and b_i on the boundary Γ into excitation electrodes by injecting a DC current of I_i Ampere at the electrode positions shown in Fig. 2 without considering the acoustic and static magnetic fields. Denote the injected current function as

$$I(\mathbf{r}) = \sum_{i=1}^{N} I_i \left[\delta(\mathbf{r} - \mathbf{r}_{a_i}) - \delta(\mathbf{r} - \mathbf{r}_{b_i})\right] \tag{2}$$

Here, $\mathbf{r}$ denotes a point in space. It is possible to derive potentials within the target that satisfy

$$\begin{cases} \nabla \cdot (\sigma \nabla u_2) = I(\mathbf{r}) \\ \sigma \frac{\partial u_2}{\partial n}\Big|_{\Gamma} = 0 \end{cases} \tag{3}$$

The corresponding current density is

$$\mathbf{J}_2 = -\sigma \nabla u_2 \tag{4}$$

Here, u_2 is the reciprocal potential, and $\mathbf{J}_2$ is the reciprocal current density.

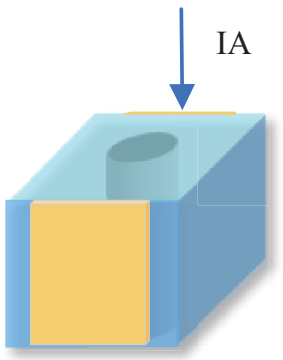

FIGURE 2. Reciprocal process of MAET.

2.3. Reconstruction Algorithm

According to the above equation, for a low conductivity target body, the total current density in the target body is:

$$\mathbf{J} = \sigma\boldsymbol{\nu} \times \mathbf{B}_0 - \sigma\nabla u_1 \tag{5}$$

From the current continuity theorem, it can be derived that the potential of the target body (u_1) satisfies the Poisson equation:

$$\nabla \cdot (\sigma\nabla u_1) = \nabla \cdot (\sigma\boldsymbol{\nu} \times \mathbf{B}_0) \tag{6}$$

The boundary conditions are:

$$\sigma \left.\frac{\partial u_1}{\partial n}\right|_{\Gamma} = \sigma\mathbf{v} \times \mathbf{B}_0 \cdot \mathbf{n}|_{\Gamma} \tag{7}$$

Since the vibration velocity $\boldsymbol{\nu}$ and the potential are functions of time, and the source of excitation in the reciprocal process is DC, the corresponding electric field is a constant current field. Bringing the above equation into the second Green's function, we have:

$$\int_\Omega u_2\nabla\cdot(\sigma\boldsymbol{\nu}\times\mathbf{B}_0)\,\mathrm{d}\Omega - \int_\Omega u_1 I(\mathbf{r})\,\mathrm{d}\Omega = \int_\Gamma \sigma u_2\mathbf{v}\times\mathbf{B}_0\cdot\mathbf{n}\mathrm{d}\Gamma \tag{8}$$

Using the Gaussian Scattering Theorem, there is:

$$\int_\Omega \nabla \cdot (u_2\sigma\boldsymbol{\nu} \times \mathbf{B}_0)\,\mathrm{d}\Omega = \int_\Gamma \sigma u_2\mathbf{v} \times \mathbf{B}_0 \cdot \mathbf{n}\mathrm{d}\Gamma \tag{9}$$

Further, there is:

$$\int_\Omega u_1 I\,(\mathbf{r})\,\mathrm{d}\Omega = \int_\Omega \mathbf{J}_2 \cdot (\mathbf{v} \times \mathbf{B}_0)\,\mathrm{d}\Omega \tag{10}$$

Substituting $I(\mathbf{r})$, we have

$$\int_\Omega u_1 I\,(\mathbf{r})\,\mathrm{d}\Omega = \sum_{i=1}^{N} u_{1a_ib_i} I_i \tag{11}$$

Therefore, there are

$$\sum_{i=1}^{N} u_{1a_ib_i} I_i = \int_\Omega \mathbf{J}_2 \cdot (\mathbf{v} \times \mathbf{B}_0)\,\mathrm{d}\Omega \tag{12}$$

Considering that there is only one pair of electrodes at a and b, and a current of unit amperage is passed through them, there are

$$u_{1ab} = \int_\Omega \mathbf{J}_2 \cdot (\mathbf{v} \times \mathbf{B}_0)\,\mathrm{d}\Omega \tag{13}$$

Here u_{1ab} is the measured voltage, and $\mathbf{J}_2$ is the current density distribution of the reciprocal process.

3. SIMULATIONS

3.1. Simulation Model Building

Finite element simulation software plays a crucial role in performing numerical simulation studies of imaging complex structural models. A two-dimensional simulation model with a complex irregularly shaped abnormal body was constructed in the simulation software, and the external model simulating normal tissue was set as a 5 cm × 5 cm square imaging area with a conductivity of 0.2 S/m. The internal abnormal body presented a complex irregular shape with a conductivity of 0.5 S/m. This design simulated the possible presence of lesions or other abnormal tissues in the biological tissues. The specific

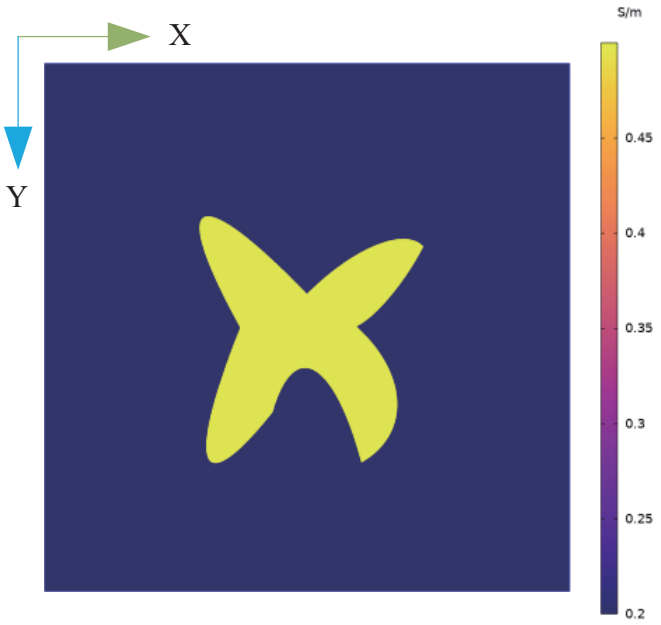

FIGURE 3. Simulation model specific parameters.

parameters of the model are shown in Fig. 3. The irregular distribution of the conductivity increases the complexity of the simulation, and it leads to changes in the scattering and absorption characteristics of the electromagnetic field in different regions.

The ultrasonic transducer as an excitation source is placed 6.5 cm from the front surface of the target body in the simulation. The excitation is performed at equal angular spacing along an arc centered on the center of the target to achieve a full scan of the target area. This configuration mimics the probe arrangement in actual ultrasound imaging and is intended to obtain more comprehensive imaging data through excitation at different angles. The design and optimization of the ultrasound transducer is crucial for improving the imaging quality and resolution [9]. Here the scanning angle is set to 200° with a step size of 25°.

3.2. MAET Forward Problem

The actual process is to solve the positive problem of MAET, which refers to solving the measured voltage on the surface of the target body with a known equivalent current source inside the target body due to the coupling of multiple physical fields. To obtain the equivalent current source, the vibrational velocity distribution of the particles inside the target body under the action of ultrasound should be obtained first. Here, the distributions of the x-component of the vibrational velocity at the moments of $t = 46.7\,\mu s$, $t = 54.3\,\mu s$, $t = 70.9\,\mu s$, and $t = 76.4\,\mu s$ are selected, as shown in Fig. 4. The upper left reflects the vibrational velocity component when the sound wave just enters the target body at the moment of $t = 46.7\,\mu s$, and the upper right reflects the vibrational velocity component when the sound wave reaches the left interface of the anomaly at the moment of $t = 54.3\,\mu s$. The lower left reflects the velocity component at $t = 70.9\,\mu s$ after the sound wave passes through the right interface of the anomaly, and the lower right reflects

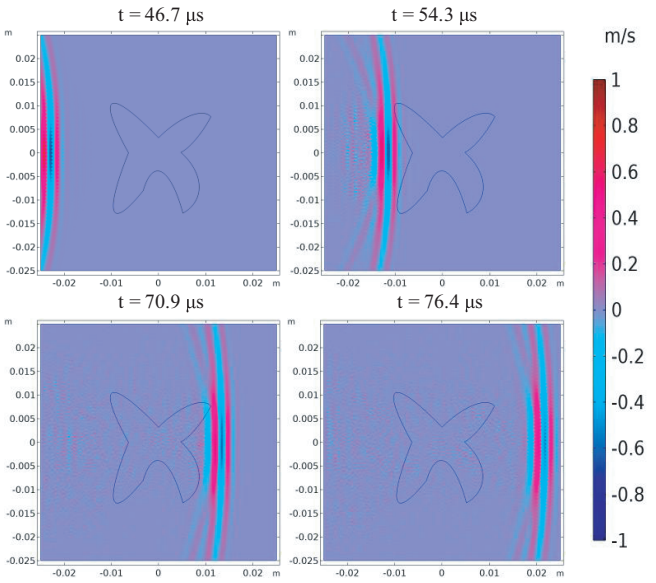

FIGURE 4. Distribution of the x-component of the vibration velocity at different moments of time.

the velocity component at $t = 76.4\,\mu s$ after the sound wave passes through the anomaly. The correctness of the velocity distribution can be verified by combining the arrival time and propagation velocity of the sound wave.

With the vibration velocity, the equivalent current source inside the target is known, and the external current density at the corresponding moment is selected for verification, as shown in Fig. 5. It can be seen that the external current density is mainly affected by the vibration velocity in the case of constant conductivity distribution and magnetic field strength, and the correctness of the simulation model can be verified by comparing Fig. 4 and Fig. 5.

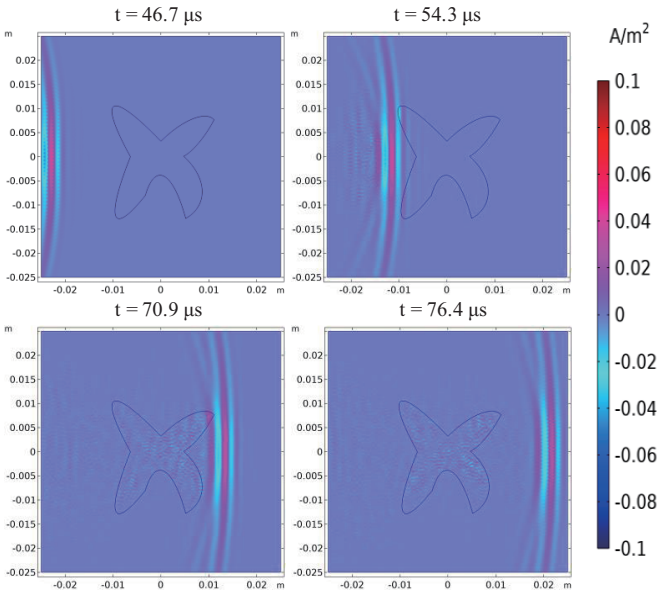

FIGURE 5. External current density distribution at corresponding moments.

3.3. Signal Analysis

The value of the voltage on the surface of the target body is obtained by solving the current source obtained from the simulation of the forward problem above. Then, the voltage data is extracted from the detection electrodes on both sides of the target body. When the ultrasonic transducer is excited along the horizontal position with the target body, the MAET signals received by the electrodes are shown in Fig. 6. It can be seen that the pulses appear at 45.7 μs and 79.3 μs corresponding to the moments when the acoustic wave arrives at the interface between the front and back of the target body. Corresponding to the irregular shape of the anomaly in the middle, the voltages can be seen as two main peaks corresponding to the moments when the acoustic wave enters and exits the anomaly. The irregular shape of the anomaly results in the appearance of multiple small pulses in the waveform of the voltage signals, as shown by the red dashed box in the figure. The polarity of the pulse peaks is affected by the interface with different conductivity gradients, positive and negative, respectively. Positive polarity indicates that the conductivity on the left side of the interface is less than that on the right side; negative polarity indicates that the conductivity on the left side of the interface is greater than that on the right side.

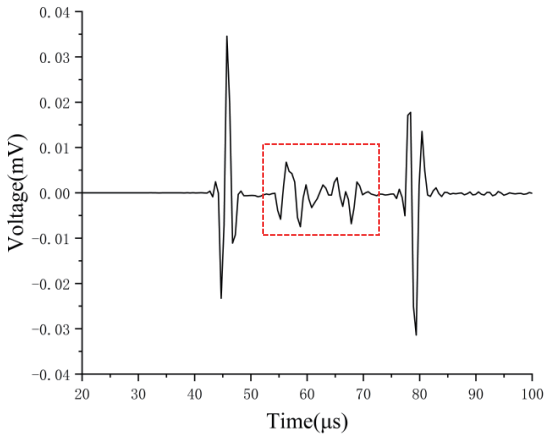

FIGURE 6. Signal of MAET.

3.4. Analysis of Imaging Results

The measured signals obtained by solving the simulation model are used for image reconstruction based on the above equation. The traditional MAET image reconstruction methods include time reversal method, and currently the commonly used reconstruction algorithms include linear back projection (LBP), Tikhonov regularization, etc. The Tikhonov regularization method is used in this paper and compared with the time reversal method to verify the advantages of the method. The time reversal method and Tikhonov regularization method are briefly introduced in the following.

Time reversal: The time reversal method is an advanced sound source reconstruction technique [13], whose core principle lies in utilizing the time reversal property of the acoustic field to achieve adaptive focusing of the sound source. Theoretically, the method is able to realize sound pressure reconstruc-

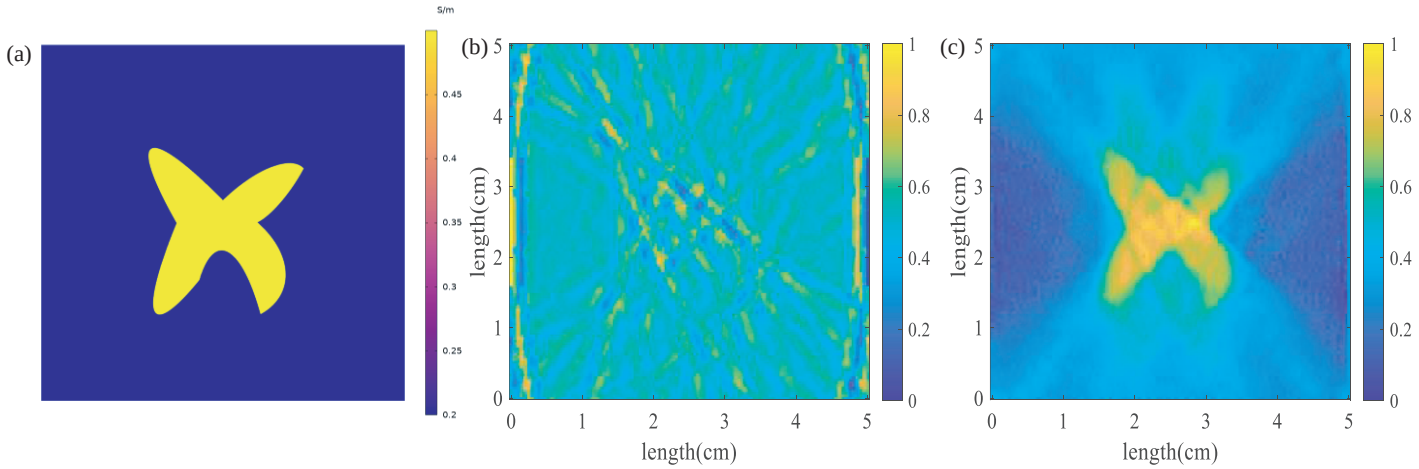

FIGURE 7. Imaging results. (a) Original image. (b) Time reversal method. (c) Tikhonov regularization.

tion at any point within the acoustic field by using the sound pressure and its normal gradient captured on the closed boundary as a secondary sound source to be re-emitted without a priori knowledge. However, in practice, since the acoustic pressure and its normal gradient cannot be acquired simultaneously, researchers have proposed an innovative approach that utilizes only the acoustic pressure information and combines it with the gradient of the Green's function to perform a time reversal process for the reconstruction of the acoustic field. The inverse problem of MAET is reduced to the inverse source problem of voltage-like fluctuations. The time reversal method is based on a derived expression for the field source ($\mathbf{r}$: field point, $\mathbf{r}'$: source point, t_{rd}: $t_{rd} = 2T_0 - t + |\mathbf{r} - \mathbf{r}'|/c_s, T_0$: Initial moment of reversal, t: Actual moment of propagation, c_0: Speed of the sound wave, c_s: Speed of sound waves in a medium):

$$H(r') = \frac{1}{2\pi c_0^2} \oint\limits_{r \in S} \mathrm{d}s \frac{\mathbf{n} \cdot (\mathbf{r}' - \mathbf{r})}{|\mathbf{r}' - \mathbf{r}|^2} \left[\frac{u'(r', t_{rd})}{|\mathbf{r}' - \mathbf{r}|} - u''(r', t_{rd})/c_0 \right] \tag{14}$$

Tikhonov regularization: The Tikhonov regularization algorithm [14] is an infinite approximation of the solution of the original problem by using a set of solutions of a suitable problem similar to the original problem, and a regularization parameter λ is used to determine the distance of the similar solution from the solution of the original problem [11]. It introduces a regularization term to the objective function of the standard linear regression model:

$$f(g) = \frac{1}{2} \|Sg - U\|_2^2 + \frac{1}{2} \lambda \|g\|_2^2 \tag{15}$$

Here, $\|g\|_2^2$ is the L2 norm of g, and λ is called the regularized intensity parameter. The selection of λ has a direct impact on the quality of image reconstruction. S is the mapping relationship, g the conductivity distribution, and U the measured voltage data. Fig. 7 shows the original true image of the above simulation model and the reconstructed image obtained with very few measurements (10 probe angles, 200 measurements per angle) using the time reversal method and the method in this paper, respectively.

The reconstructed image after normalization can be seen in the above figure, and the reconstructed conductivity of the anomalies is significantly higher than that of the normal part. In addition, the normalized setting of the reconstructed conductivity can be set by simulating the anomalous body with a larger value of conductivity, so that more accurate conductivity information can be obtained. In the field of image quality assessment, traditional evaluation methods usually focus on quantifying the differences between the reference image and the image to be evaluated. However, these methods tend to ignore the ability of the Human Visual System (HVS) to recognize structural information in images in image quality perception. Therefore, evaluation metrics that can mimic the characteristics of HVS, especially when distinguishing between sample images and reference images, will show higher accuracy and relevance. Given the sensitivity of HVS to the structural features of images, the Structural Similarity (SSIM) metric was developed [15]. The value of this metric ranges between -1 and 1. The closer the value is to 1, the more similar the two images are.

The SSIM values of the images obtained from different reconstruction algorithms in the above figure are compared below and presented in Table 1.

TABLE 1. Comparison of SSIM values for different algorithms.

reconstruction algorithms	SSIM
Time reversal	0.489
Tikhonov regularization	0.649

It can be seen that the SSIM value of Tikhonov regularization is much closer to 1 for the same collected data. This indicates that for complex structural models, the Tikhonov regularization method is better than the time reversal method. Therefore, for complex structural models, it is more advantageous to reconstruct the image using the Tikhonov regularization method based on the method in this paper.

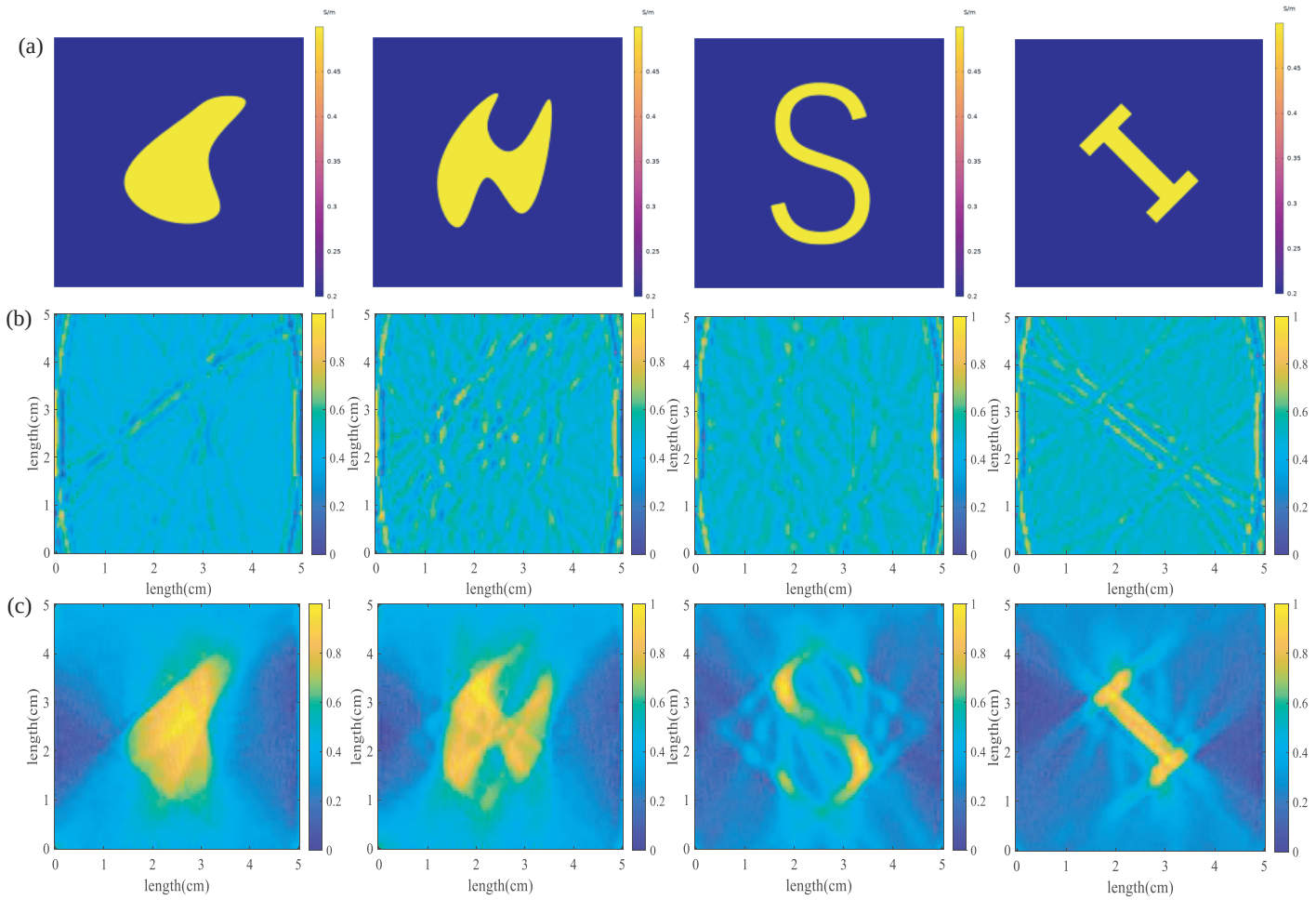

FIGURE 8. Reconstructed image of a single complex structural anomaly Blue areas are normal tissue with a conductivity of 0.2 S/m. Yellow areas are abnormal bodies with a conductivity of 0.5 S/m. (a) original image, (b) reconstruction from the time reversal method, (c) reconstruction using Tikhonov regularization.

3.5. Further Validation of Complex Structural Models

3.5.1. Single Complex Structural Anomaly

Figure 8 shows the reconstructed images for different single complex structure simulation models based on the method of this paper using the Tikhonov regularization method. It can be seen that it is almost impossible for conventional imaging methods to reconstruct the original image with little measurement data, and only the fuzzy boundary is vaguely visible. The algorithm in this paper not only reconstructs the uniform conductivity distribution information at the boundary and inside of the target body, but also solves the problem of poor reconstruction effect of the traditional method in the case of underdetermined data. More importantly, the method in this paper can accurately and reliably reconstruct the conductivity of complex structural models.

3.5.2. Multiple Anomalies

Above are reconstructed images of different simulation models of individual complex structures. However, in real 2D modeling situations, complex structures not only stem from their irregular geometry, but also greatly increase the complexity of the model when there are a large number of anomalies. Likewise, for 3D modeling, multiple complex three dimensional shapes greatly complicate the reconstruction. When there are multiple anomalies in the imaging area, the quality of the received signal also deteriorates due to the influence of echoes between the interfaces, which increases the complexity of the solution. Considering this factor, the multiple anomalies model is set up for verification. As shown in Fig. 9, it can be seen that the method proposed in this paper still has the above advantages under the premise that the presence of multiple anomalies leads to poor signal.

3.5.3. Anomalies with Multiple Gradients of Conductivity

Complex structural models for irregular geometries with multiple anomalies were considered. For further validation, a conductivity multi-gradient model, where the anomalies have a layered rather than a single conductivity distribution inside, was considered to simulate biological tissues. The model conductivity distribution and the imaging results of different algorithms are shown in Fig. 10. It can be seen that the method

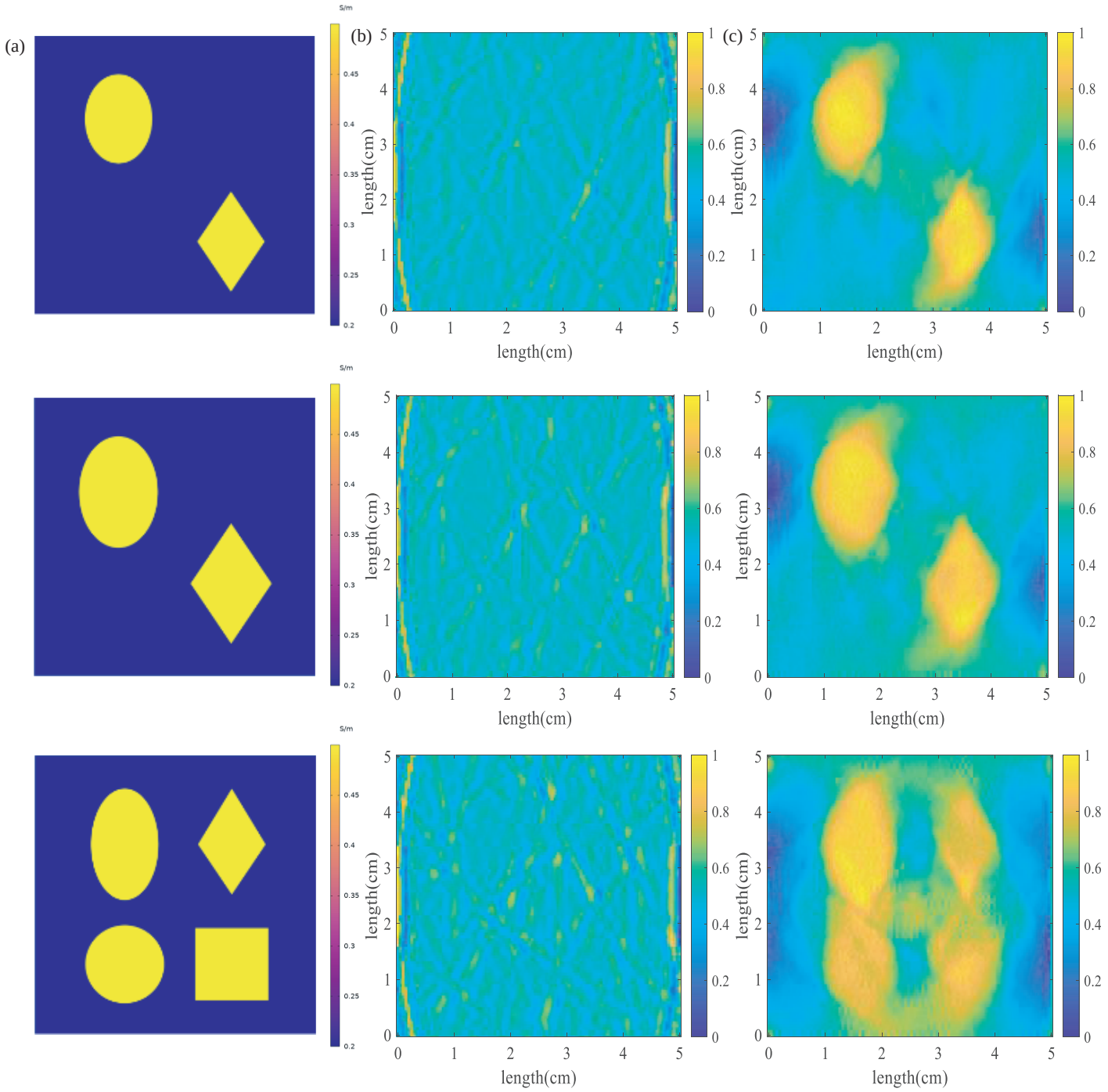

FIGURE 9. Reconstructed image of multiple anomalies Blue areas are normal tissue with a conductivity of 0.2 S/m. Yellow areas are abnormal bodies with a conductivity of 0.5 S/m. (a) Original image, (b) reconstruction from the time reversal method, (c) reconstruction using Tikhonov regularization.

proposed in this paper still shows significant improvement over the standard method.

4. EXPERIMENTS

4.1. Production of the Phantom

In order to further verify the validity and stability of the complex structure model imaging proposed in this paper, experimental verification was carried out by fabricating gel phantoms in the laboratory. The shape and size of the phantoms are shown in Fig. 11. The conductivity of the phantom was 0.3 S/m, and transformer oil was placed in the hollow part to simulate the anomalies. Two groups of complex structure phantoms were constructed. One group was a multi-anomaly distribution with up to four anomalies, see Figs. 11(a), (b), and the other group

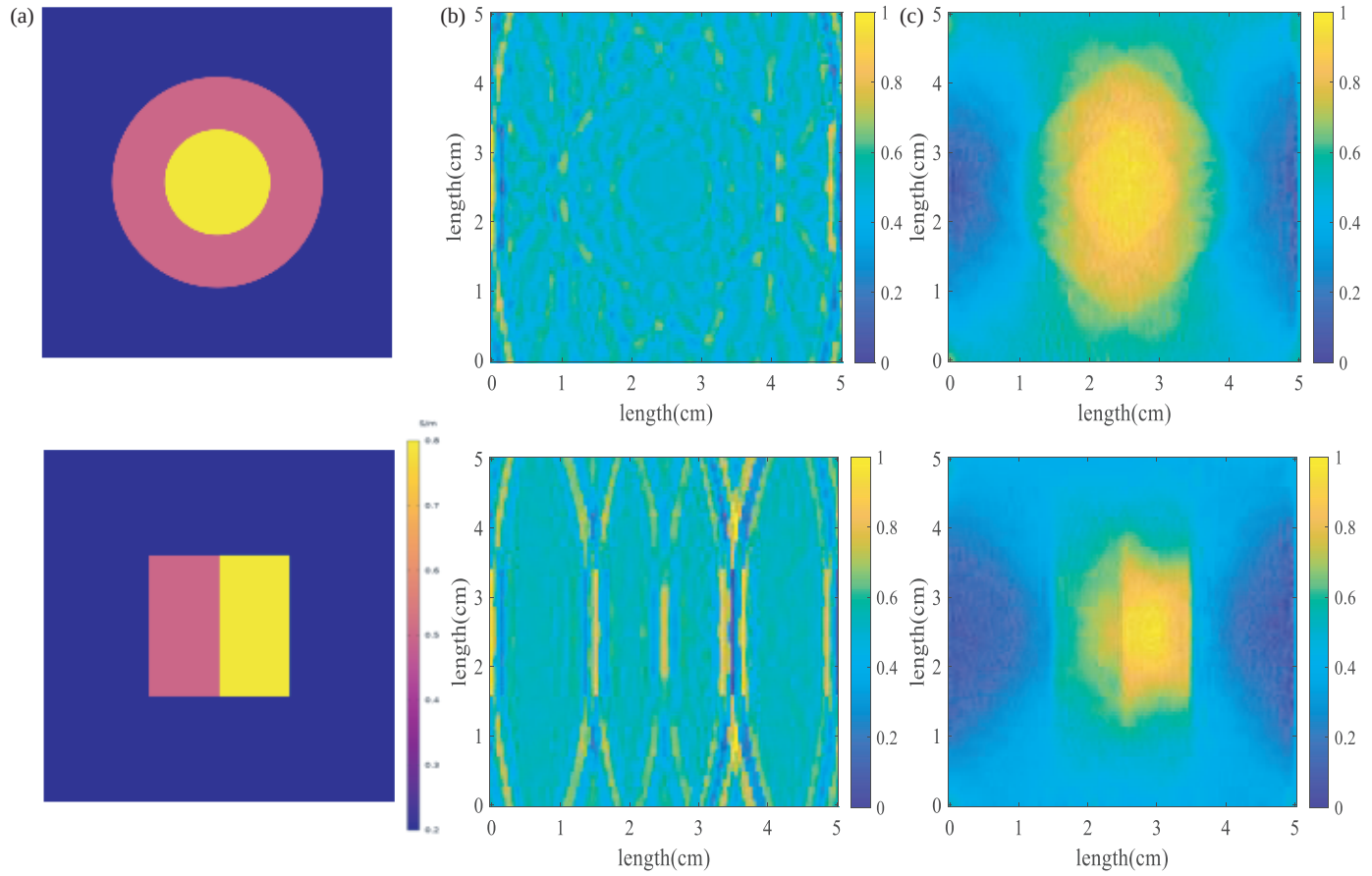

FIGURE 10. Reconstructed images of anomalies with multiple gradients of conductivity Blue areas are normal tissue with a conductivity of 0.2 S/m. Yellow areas are abnormal bodies with a conductivity of 0.5 S/m. (a) Original image, (b) reconstruction from the time reversal method, (c) reconstruction using Tikhonov regularization.

FIGURE 11. Shape and size of the phantoms.

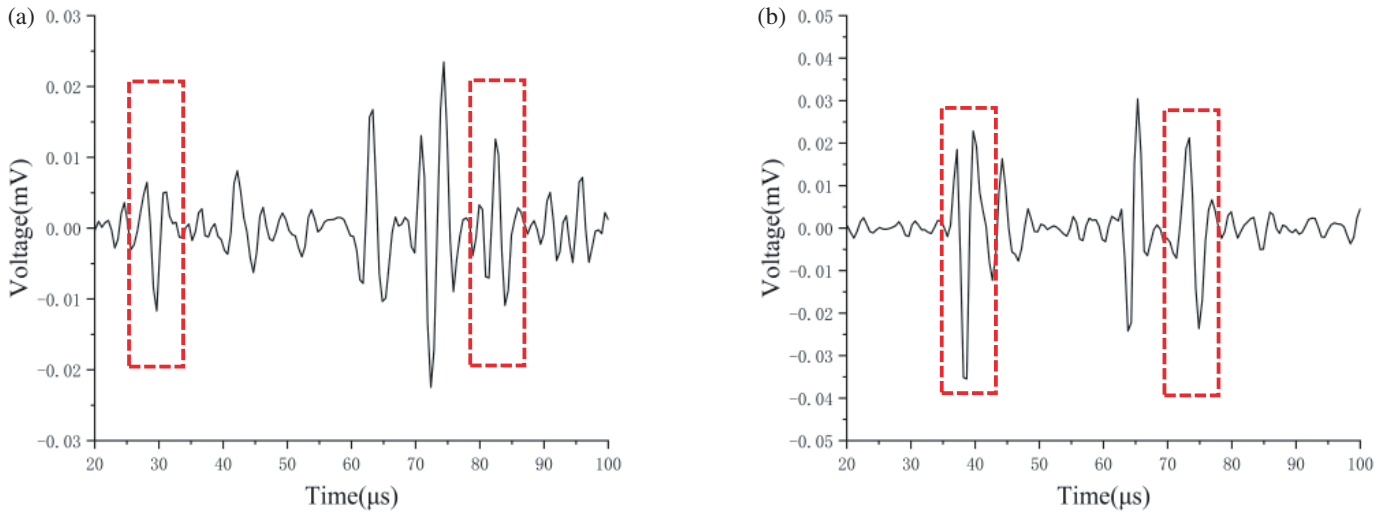

FIGURE 12. Signal of the MAET in the experiment ((a) four anomalies, (b) irregular anomalies).

was an irregularly shaped anomaly distribution, see Figs. 11(c), (d). The ultrasonic transducer frequency was 1 MHz.

4.2. Experimental Procedure and MAET Signal

The MAET system we built includes signal generators, signal amplifiers, ultrasonic transducers, mobile control units, permanent magnets, measurement electrodes, signal filters, acquisition cards, and oscilloscopes. After the preparation of the phantom is completed, it is put into the experimental device. During the experiment, the ultrasound probe is scanned along a circular arc with the center of the imaging area as the origin and the probe distance as the radius, and the scanning mode is consistent with the simulation. After the scanning is finished, the signal analysis of MAET is carried out according to the electrical signals received by the detection electrodes. Since the actual signal is interspersed with low-frequency and high-frequency noise, the signal is first passed through a Butterworth bandpass filter. The Butterworth filter is characterized by a maximally flat frequency response curve with no undulation in the passband and a gradual decrease to zero in the stopband, which serves to effectively filter out unwanted frequency components to achieve clear signal transmission and processing while ensuring that the signal in the passband is not distorted. The filtered signal is analyzed as shown in Fig. 12. The left side is the MAET signal corresponding to the distribution of four anomalies, and the right side is the MAET signal corresponding to the distribution of irregular anomalies. In the red dashed box are the different polarity pulses reflecting the front and back interfaces, and the pulse signals in the middle reflect the anomalous body location and conductivity information. In contrast to the simulated signals in Fig. 6, the experimental signals in Fig. 12 also reflect the interfaces on the left and right sides where conductivity produces changes as well as the signals in the middle reflecting information about the distribution of the anomalies. The results show a high degree of consistency between the experimental and simulated signals, demonstrating the feasibility of further applying the method proposed in this paper to practical applications, thus enabling a more comprehensive reflection of anomaly information.

5. CONCLUSIONS

In this paper, we utilize a proposed MAET method for conductivity reconstruction of complex structural models for simulation analysis and experimental validation. The conductivity distribution of anomalies in complex structural models is reconstructed in simulation by this algorithm, and the advantages of our proposed method are verified by comparing it with the real conductivity distribution and traditional reconstruction methods. Finally, consistency between experimental and simulated signals suggest that the feasibility and effectiveness of the proposed method may also apply to experiments. This will be verified in future work. The proposed method has the following advantages:

The MAET method for conductivity reconstruction of complex structural models proposed in this paper reconstructs the conductivity distribution information at the boundaries and inside the target body, no longer imaging only the boundaries where the conductivity changes. While the distribution information of the anomalous body is enhanced, the image resolution and structural similarity are improved. The method is suitable for the conductivity reconstruction of complex structural targets with irregular shapes and multi-gradient conductivity distributions, and can be extended to a variety of industrial and medical applications for complex structures.

ACKNOWLEDGEMENT

This work was supported in part by the National Natural Science Foundation of China under Grant Nos. 52377227, 52007182, 52277233, 52377018.

REFERENCES

[1] Guo, C., Y. Chen, and J. Li, "Radiographic imaging and diagnosis of spinal bone tumors: Alexnet and resnet for the classification of tumor malignancy," *Journal of Bone Oncology*, Vol. 48, 100629, 2024.

[2] Grasland-Mongrain, P. and C. Lafon, "Review on biomedical techniques for imaging electrical impedance," *IRBM*, Vol. 39, No. 4, 243–250, 2018.

[3] Wen, H., J. Shah, and R. S. Balaban, "Hall effect imaging," *IEEE Transactions on Biomedical Engineering*, Vol. 45, No. 1, 119–124, 1998.

[4] Wen, H., "Feasibility of biomedical applications of Hall effect imaging," *Ultrasonic Imaging*, Vol. 22, No. 2, 123–136, 2000.

[5] Zeng, X., G. Liu, H. Xia, and X. Xu, "An acoustic characteristic study of magneto-acousto-electrical tomography," in *2010 3rd International Conference on Biomedical Engineering and Informatics*, Vol. 1, 95–98, Yantai, China, Oct. 2010.

[6] Kunyansky, L., "A mathematical model and inversion procedure for magneto-acousto-electric tomography," *Inverse Problems*, Vol. 28, No. 3, 035002, 2012.

[7] Salim, M. I. M., E. Supriyanto, J. Haueisen, I. Ariffin, A. H. Ahmad, and B. Rosidi, "Measurement of bioelectric and acoustic profile of breast tissue using hybrid magnetoacoustic method for cancer detection," *Medical & Biological Engineering & Computing*, Vol. 51, 459–466, 2013.

[8] Zengin, R. and N. G. Gençer, "Lorentz force electrical impedance tomography using magnetic field measurements," *Physics in Medicine & Biology*, Vol. 61, No. 16, 5887, 2016.

[9] Sun, T., X. Zeng, P. Hao, C. T. Chin, M. Chen, J. Yan, M. Dai, H. Lin, S. Chen, and X. Chen, "Optimization of multi-angle magneto-acousto-electrical tomography (MAET) based on a numerical method," *Mathematical Biosciences and Engineering*, Vol. 17, No. 4, 2864–2880, 2020.

[10] Jin, Y., H. Zhao, G. Liu, H. Xia, and Y. Li, "The application of a wavelet filtering method in magneto-acousto-electrical tomography," *Physics in Medicine & Biology*, Vol. 68, No. 14, 145014, 2023.

[11] Cheng, Z., Z. Sun, J. Wang, and K. Jia, "Magneto-acousto-electrical tomography using nonlinearly frequency-modulated ultrasound," *Physics in Medicine & Biology*, Vol. 69, No. 8, 085014, 2024.

[12] Lorentz, H. A., "The theorem of poynting concerning the energy in the electromagnetic field and two general propositions concerning the propagation of light," *Amsterdammer Akademie der Wetenschappen*, Vol. 4, 176, 1896.

[13] Preston, C., A. M. Alvarez, M. Allard, A. Barragan, and R. S. Witte, "Acoustoelectric time-reversal for ultrasound phase-aberration correction," *IEEE Transactions on Ultrasonics, Ferroelectrics, and Frequency Control*, Vol. 70, No. 8, 854-864 2023.

[14] Liu, Z., X. Tan, and W. Jia, "An image reconstruction algorithm based on Tikhonov regularization in electromagnetic tomography," in *2010 International Conference on Measuring Technology and Mechatronics Automation*, Vol. 1, 488–491, Changsha, China, Mar. 2010.

[15] Dziembowski, A., W. Nowak, and J. Stankowski, "IV-SSIM — The structural similarity metric for immersive video," *Applied Sciences*, Vol. 14, No. 16, 7090, 2024.